Published in final edited form as:
Dev Cell. 2012 September 11; 23(3): 573–586. doi:10.1016/j.devcel.2012.08.002.

Lipid-sorting by ceramide structure from plasma membrane to ER for the cholera toxin receptor ganglioside GM1

Daniel J.-F. Chinnapen[1,3], **Wan-Ting Hsieh**[5], **Yvonne M. te Welscher**[1], **David E. Saslowsky**[1,3,4], **Lydia Kaoutzani**[1], **Eelke Brandsma**[1], **Ludovic D'Auria**[1], **Hyejung Park**[9], **Jessica S. Wagner**[1,4], **Kimberly R. Drake**[7], **Minchul Kang**[7], **Thomas Benjamin**[2,3], **M. David Ullman**[6], **Catherine E. Costello**[9], **Anne K. Kenworthy**[7,8], **Tobias Baumgart**[5], **Ramiro H. Massol**[1,3,4], and **Wayne I. Lencer**[1,3,4,*]

[1]Division of Gastroenterology, Children's Hospital, Boston, MA 02115, USA

[2]Department of Pathology, Boston, MA 02115, USA

[3]Harvard Medical School, Boston, MA 02115, USA

[4]Harvard Digestive Diseases Center, Boston, MA 02115, USA

[5]Department of Chemistry, University of Pennsylvania, Philadelphia, PA 19104, USA

[6]Department of Veterans Affairs, VA Medical Center, 200 Springs Road, Building 17, Bedford, MA 01730, USA

[7]Department of Molecular Physiology and Biophysics, Vanderbilt University, Nashville, Tennessee 37232

[8]Department of Cell and Developmental Biology, Vanderbilt University, Nashville, Tennessee 37232

[9]Department of Biochemistry, Boston University School of Medicine, Boston Massachusetts 02118

SUMMARY

The glycosphingolipid GM1 binds cholera toxin (CT) on host cells and carries it retrograde from the plasma membrane (PM) through endosomes, the *trans*-Golgi (TGN), and the endoplasmic reticulum (ER) to induce toxicity. To elucidate how a membrane lipid can specify trafficking in these pathways, we synthesized GM1 isoforms with alternate ceramide domains and imaged their trafficking in live cells. Only GM1 with unsaturated acyl chains sorted efficiently from PM to TGN and ER. Toxin binding, which effectively crosslinks GM1 lipids, was dispensable, but membrane cholesterol and the lipid raft-associated proteins actin and flotillin were required. The results implicate a protein-dependent mechanism of lipid-sorting by ceramide structure and provide a molecular explanation for the diversity and specificity of retrograde trafficking by CT in host cells.

*Correspondence: wayne.lencer@childrens.harvard.edu; (t) 617-919-2573; (f) 617-730-0495. 300 Longwood Avenue, Enders Bldg. RM 609, Boston, MA 02115.

The authors report no conflict of interests.

INTRODUCTION

Cholera toxin typifies the AB_5-subunit toxins that have co-opted a lipid-based, rather than a protein-based, receptor to traffic retrograde from the PM through endosomes and TGN into the ER of host cells for the induction of disease (Johannes and Popoff, 2008; Lencer and Tsai, 2003; Sandvig et al., 1992; Spooner and Lord, 2012). The lipid receptor that binds CT at the cell surface and is required for toxin entry into the endosome and sorting to the ER is the ganglioside GM1 (Cuatrecasas, 1973), but how GM1 can act as the sorting vehicle for toxin trafficking in these pathways is not understood.

Gangliosides are acidic glycosphingolipids comprised of a complex extracellular oligosaccharide that binds the toxins and a ceramide domain that anchors the lipid in the membrane bilayer. The oligosaccharide traps the gangliosides in the outer-leaflet of cell membranes (trans-leaflet “flip-flop” is very slow)(Cantu et al., 2011). There is no evidence for transfer of the gangliosides between organelles of intact cells by cytosolic lipid transfer proteins, and they are transported to different intracellular destinations by vesicular traffic (Brown and Mattjus, 2007; Neumann and van Meer, 2008). Both the oligosaccharide and the ceramide domains of naturally-occurring glycosphingolipids exhibit various degrees of structural heterogeneity (Hakomori, 2003). In human intestinal T84 cells, the predominant GM1 species have ceramide chains with C24:0, C24:1, C16:0 and C16:1 fatty acids (Lencer and Costello unpublished data). In this cell line, not all gangliosides that bind the AB_5 subunit toxins by their oligosaccharide domain traffic from PM to ER, suggesting that the ceramide domain might dictate their native sorting pathways (Fujinaga et al., 2003; Wolf et al., 1998). In support of this hypothesis, there is evidence that the ceramide structure of sphingomyelin acts as a determinant for trafficking into late endosomes and lysosomes (Gupta et al., 2010; Koivusalo et al., 2007); and when incorporated into HeLa cells, GM1 ceramides containing the unsaturated C18:1 fatty acid allow for greater CT toxicity (Masserini et al., 1990).

Two mechanisms are proposed to explain lipid sorting in mammalian cells. Both propose a key dependence on lipid structure. One invokes a molecular sorting process in which individual lipids segregate in membranes of different contours and compositions as determined by the structure of the lipid (molecular shape) and driven by the minimal free energy of the space it occupies in the membrane bilayer (Mukherjee et al., 1999), though some studies provide evidence against this as a sole mechanism of action (Romer et al., 2010; Sorre et al., 2009; Tian et al., 2009). With respect to GM1, this model predicts that the GM1 species with kinked unsaturated chain ceramides would energetically favor partition into the curved membrane contours of sorting tubules that emanate from the endosome and thus sort to non-lysosomal intracellular destinations including the ER. The GM1 species with long straight saturated chain ceramides, however, would prefer flat membranes and remain in the endosome maturing along the degradative pathway. The other model invokes a cooperative sorting process involving self-assembly of certain lipids into membrane “nanodomains” (often termed lipid rafts) based on lipid phase behavior and subsequent interactions with other membrane components (Jacobson et al., 2007; Kaiser et al., 2009; Lingwood and Simons, 2010; Sorre et al., 2009; Tian et al., 2009). The nanodomains formed are dependent on associated protein scaffolds and links to the actin cytoskeleton for biological function (Lingwood et al., 2008; Romer et al., 2010; Sharma et al., 2004). Sphingolipids containing long saturated chain fatty acids that phase segregate in liquid ordered (L_o) domains of artificial membranes are considered essential structural components, along with cholesterol. The glycosphingolipids (and sphingomyelin) fall within this group (Lingwood and Simons, 2010), and there is evidence that these lipids sort the AB_5 toxins retrograde from PM to ER by association with lipid rafts (Falguieres et al., 2001; Fujinaga et al., 2003; Orlandi and Fishman, 1998; Smith et al., 2006; Wolf et al., 1998).

In this paper, we test the hypotheses that a subset of the GM1 sphingolipids traffic naturally from PM to ER, and that ceramide structure explains the specificity of lipid sorting into this pathway. To do this, we synthesized GM1 species with identical fluorophore-labeled oligosaccharide head groups but with different ceramide domains and examined their intracellular trafficking in live cells after incorporation into the PM. The GM1 species prepared were predicted to discriminate between liquid ordered (L_o) and liquid disordered (L_d) lipid phases in artificial membranes (Lingwood and Simons, 2010), and between membranes with different phase-characters and contours *in vivo* (Kaiser et al., 2009; Lingwood et al., 2009; Mukherjee et al., 1999; Simons and Gerl, 2010), thus allowing for inferences on the mechanisms of lipid sorting.

Importantly, we studied trafficking of the GM1 sphingolipids in the presence and absence of CT. CT binds to GM1 via the toxin's homopentameric B-subunit, which scaffolds up to five GM1 molecules together. Such clustering of the glycosphingolipids by the AB_5 toxins structurally remodels both artificial and native cell membranes to form nanodomains and in some cases membrane tubulations (Johannes and Mayor, 2010; Panasiewicz et al., 2003; Romer et al., 2007; Romer et al., 2010; Safouane et al., 2010; Tian et al., 2009). Thus, the AB_5 toxins can induce their own trafficking platform and strongly affect the membrane dynamics of their lipid receptors in ways that could explain their ability to enter the ER and intoxicate host cells. On the other hand, CT retains toxicity when only one or two GM1 sphingolipids are bound (Wolf et al., 2008), suggesting a native pathway for glycosphingolipid trafficking (Lencer and Tsai, 2003; Wolf et al., 1998).

RESULTS

Synthesis and characterization of GM1 variants

We synthesized different molecular species of GM1 with or without polar Alexa Fluors® coupled to the oligosaccharide head-group and with the following fatty acyl chains in the ceramide domain: C12:0, C16:0, C16:1, and C18:0 (Figure 1A). All structures were confirmed by mass spectrometry (Supplemental Experimental Procedures, Table S1 and Figure S1). With the exception of the C12:0 molecular species, all are naturally-occurring lipids (Hakomori, 2003; Nilsson and Svennerholm, 1982). The Alexa-labeled GM1 lipids still bound CTB specifically but with about 10-fold apparent lower affinity as compared to unlabeled GM1 (data not shown). The phase-partitioning behavior of the GM1 variants was defined by reconstituting selected GM1 species into a series of giant unilamellar vesicles (GUVs) containing lipid:sterol compositions that model biological membranes with a large range of co-existing liquid-disordered (L_d) and liquid-ordered (L_o) phases at room temperature (Figure 1D). Phase partitioning of the GM1 variants was visualized by confocal microscopy using Texas red® 1,2-dihexadecanoyl-*sn*-glycero-3-phosphoethanolamine (TR-DHPE) to mark the L_d phase (Figures 1B & 1C). Fifty vesicles were imaged for each GM1 isoform, and phase partitioning of the ganglioside alone or when clustered together as a GM1-CTB complex was assigned to be primarily L_o, L_d, or non-preferential (NPP) by quantitative image analysis as previously described (Methods and (Johnson et al., 2010)).

In the absence of crosslinking by CTB, we found that the C12:0-GM1 and C18:0 fluorophore-labeled species displayed no phase preference (NPP) under some conditions, or partitioned under other conditions preferentially into the L_d or L_o phases respectively (Figure 1C). When these GM1 species were cross-linked by binding CTB, however, both partitioned almost exclusively in L_o domains under all conditions. In stark contrast, when GUVs contained the unsaturated GM1-C16:1 species and cross-linked by CTB, this lipid partitioned almost exclusively with L_d domains. Thus, GM1 with differing ceramides showed distinct phase-partitioning behaviors in GUVs, behaving largely as predicted for saturated and unsaturated lipids (Brown et al., 2000). Clustering the saturated C12:0- and

C18:0-GM1 molecules together by binding to CTB enhanced partitioning into L_o domains, consistent with previous studies on CTB-GM1 complexes (Hammond et al., 2005; Johnson et al., 2010). For the C16:1-GM1 species, however, no L_o phase partitioning was detected after CTB binding, indicating that the unsaturated ceramide has a dominant influence on phase partitioning of GM1 in GUVs.

Influence of ceramide structure on GM1 trafficking

GM1 trafficking was studied in live human epithelial A431 cells expressing EGFP-fusions to Rab5, Rab11a, and Rab7 GTPases to mark the early sorting (SE), recycling (RE), and late endosomal compartments (LE) and EGFP-fusions to Golgin97 and Sec61α to mark the TGN and ER, respectively (schematic of retrograde pathways, Figure 1E). Cells were pre-treated with Alexa-labeled or unlabeled GM1 at 10°C to preload the PM, washed in 10% fetal bovine serum at 10°C to remove free GM1, and warmed to 37°C for 60 min to allow internalization (Supplemental Methods). Conditions for loading the cells equally with the different GM1 species were determined by measures of total cell fluorescence. For the C16:0 and C16:1 pair, this was confirmed by FACS analysis of GM1 loaded cells before and after treatment with trypsin, which also showed that >83% of these Alexa-labeled GM1 lipids were incorporated into the membrane bilayer (Figure S1C and (Schwarzmann, 2001)). Confocal FRAP studies confirmed that the exogenously applied Alexa-GM1 species diffused at rates and with mobile fractions as expected for lipids in membrane bilayers as shown for the fluorescent lipid analog $DiIC_{16}$ (Figures 1F & S1D–S1E). This is distinct from the slow membrane diffusion of CT bound to endogenous GM1 (Alexa-CTB) described before (Kenworthy et al., 2004).

After switching to physiologic temperatures, we quantified the fraction of Alexa-GM1 species occupying each sub-cellular compartment in three dimensions relative to the total GM1 incorporated into the cell using the Manders colocalization coefficient (termed M_x, method as described (Tzaban et al., 2009)). Colocalization was also quantified using the Pearson's correlation coefficient (Rr). At 60 min, GM1 with short chain C12:0 and unsaturated C16:1 ceramides localized to the PM, RE, LE, and the *trans*-Golgi network (TGN) (Figures 2A, 2B & S2). On average, about 10% was associated with the TGN, 65% remained in the "recycling pathway" (PM, SE and RE), and a smaller amount (approximately 25% for C16:1) localized to late endosomes. In contrast, the saturated long chain C18:0 species localized overwhelmingly to Rab7 late endosomes (LE, 80%) (Figure S2), and none was detected in the TGN. Like the unsaturated C16:1-GM1 species, the chain-length matched but saturated C16:0-GM1 species was present in the PM and all endosomal compartments, but with greater colocalization with the LE and less with the RE as measured by the Pearson's algorithm (Figure 2A, compare left and right panels, and histograms). Most importantly, no saturated C16:0-GM1 species co-localized with the TGN (Figure 2B). Thus, only the unsaturated C16:1-GM1 and short-chain C12:0-GM1 species appeared to enter the retrograde pathway.

Trafficking of both these lipids into the TGN was completely blocked in cells pre-treated with Brefeldin A prior to GM1 incorporation (Figure 2C, data for GM1-C16:1 not shown) showing that GM1 transport was by vesicular traffic and along the PM-TGN-ER retrograde pathway exploited by CT (Fujinaga et al., 2003). We also examined the cells 5 min after warming to 37°C. At this time, a fracti on of both the C12:0- and C18:0-GM1 lipids were co-localized with Rab5 (Figure 2D), suggesting that the different molecular species transit the early endosomes *en route* to the RE, TGN, and LE, respectively.

To assay for GM1 transport into the ER, we allowed overnight uptake of the Alexa-labeled species C16:0-GM1 and C16:1-GM1 into A431 cells and counted cells positive for the presence of GM1 in the entire nuclear envelope visualized by Sec61α-EGFP (Massol et al.,

2004; Saslowsky et al., 2010). This was assessed by three investigators blinded to each other and treatment groups. Only GM1 with C16:1 unsaturated ceramides were consistently present in the ER (Figures 3A & 3B). The same results were obtained in EGFP-Sec61α expressing African green monkey kidney Bsc1 cells (Figures S3A & S3B).

Control studies showed that labeling GM1 with structurally different fluorophores (schematic Figure 1A) had no effect on the intracellular distribution of the sphingolipids as long as the fluorophore attached was strongly polar (Figure S2B). Labeling the C18:0-GM1 with the hydrophobic fluorophore BODIPY altered trafficking of this lipid (data not shown). To test whether one or another of the exogenous GM1 variants might have nonspecific toxic effects that could explain the different trafficking patterns, we loaded cells with both GM1-C18:0 and GM1-C12:0 species labeled with different polar fluorophores (Figure 1A) and examined the distribution of both lipids at 60 minutes in single cells. The two GM1 variants again sorted into distinct compartments (Figure S2C), as in cells loaded with each GM1 species alone (Figures 2A, 2B). Thus, neither lipid affected trafficking of the other.

These studies show that mammalian cells sort single GM1 molecules retrograde from PM to TGN and ER, or from PM to LE, with the structure of the ceramide domain dictating the different trafficking pathways. Remarkably, we find that only the unsaturated species of the C16-carbon ceramide pair was efficiently sorted retrograde from PM to TGN and ER. The short-chain GM1-C12:0 species was also sorted into the TGN, but this species is not a physiologic lipid and may be missorted. To test if unsaturated fatty acids in the ceramide domain might be a general rule for retrograde lipid sorting, we synthesized an additional Alexa-labeled GM1 species containing the C18:1 fatty acid (see Methods). A fraction of this GM1 variant also localized to the TGN (Figure 2B, bottom panels). Thus, it is the unsaturated-ceramide GM1 species displaying predominantly L_d behavior in artificial membranes (Figure 1) that traffic retrograde into the ER, suggesting that they are the functional toxin receptors *in vivo*.

Effect of toxin binding on GM1 trafficking

Because CT binds multiple GM1 molecules and effectively crosslinks GM1 to remodel cell membranes, we sought to determine if toxin binding might affect the intracellular sorting of the different GM1 species. As all cells expressing GM1 are sensitive to intoxication by CT, we hypothesized that clustering GM1 by toxin binding might induce retrograde TGN and ER transport for the long saturated GM1 species, which on their own did not efficiently enter the retrograde pathways. Studies in A431 cells, however, showed no such effect. Toxin binding did not divert the GM1 species containing long saturated ceramide domains (C16:0- and C18:0-GM1) from the LE to the TGN (Figure 4B, bottom panels, and Figure 4E, data not shown for C18:0-GM1). For all other GM1-species, however, there was a strong effect of toxin binding on retention of GM1 in the recycling system. We found that after binding CTB the bulk of all short/unsaturated GM1 species including C16:0, C16:1 and C12:0 (about 70–80% in each case) was no longer in the recycling compartments (PM, SE or RE); instead, it was in the LE (Figures 4A–D). Remarkably, TGN sorting was preserved for the unsaturated C16:1-GM1 species, despite the dramatic redistribution of this lipid from the RE to LE after cross-linking by CTB (Figures 4A & 4E). To test whether endogenous GM1 in A431 cells could have confounded these results, we repeated these experiments using mouse embryonic fibroblasts lacking GD2-synthase (Yamashita et al., 2003), termed here “MEF-$GM1^{-/-}$ cells”, which are completely devoid of endogenous gangliosides. Identical results were obtained (Figures 4F–4I).

To interpret this result we needed to define in more detail the pathway for transport of the unsaturated C16:1-GM1 species from PM into the TGN after binding CTB. One possibility was that the unsaturated GM1-CTB complex entered the LE but then was diverted to the

TGN via the mannose-6-phosphate receptor (Man-6-PR) retrieval pathway. This pathway, however, would not be consistent with published evidence that CT and the other AB_5 toxins take a direct route from the early sorting endosome to the TGN, bypassing the LE (Mallard et al., 1998). Another possibility was that CTB-induced crosslinking of C16:1-GM1 lipids selectively affected sorting mechanisms in the endosome, facilitating sorting into the LE pathway but having no effect on the sorting mechanism responsible for GM1 traffic to the TGN and presumably ER.

We addressed this problem by using RNAi in A431 cells against rab9 to inhibit the LE to TGN (Man-6-PR) pathway, and RNAi against syntaxin6 to inhibit the SE/RE to TGN pathway (Ganley et al., 2008; Mallard et al., 1998). In cells lacking Rab9, the CTB-GM1-C16:1 complex entered the TGN in the same amounts as in untreated cells (Figures 5A-5C). In cells lacking Syntaxin 6, however, the complexes entered the TGN with lower efficiency or not at all (Figures 5D – 5F). Thus, a fraction of the unsaturated CTB-C16:1-GM1 complexes trafficked directly from SE into the TGN, even though the bulk of these CTB crosslinked-lipids were diverted to the LE after binding CTB. This result implies a sorting step localized to the endosome that either retains GM1 lipids in the recycling system, directs the cross-linked unsaturated C16:1-GM1 lipids retrograde towards the TGN, or directs them towards the LE.

GM1 with unsaturated ceramides are functional toxin receptors

To examine ER transport of the CTB crosslinked lipids we used MEF-GM1$^{-/-}$ cells stably expressing Sec61α-EGFP. The cells were loaded at 10 °C with either t he Alexa568-labeled C16:0- or C16:1-GM1 molecular species, and then treated or not treated with Alexa647-labeled CTB, washed as described, and warmed to 37 °C for 5 h before imaging live. Transport of the CT-GM1 complexes into the ER was measured as the fraction of cells containing both GM1 and CTB co-localized with EGFP-Sec61α at the nuclear envelope and in reticular structures throughout the cytosol, again as assessed independently by three investigators. First, we found that CTB in the Sec61α compartment was always co-localized with GM1, providing evidence that GM1 remains associated with CT all the way from PM into the ER (Figure 6A). Second, we found that the CTB-C16:1-GM1 complexes moved from PM into the ER much more efficiently than the CTB-C16:0-GM1 complexes (>90% vs. <25% of cells counted, Figure 6B), exactly as predicted by the trafficking patterns of the single lipids. We also measured ER transport of GM1 in MEF GM1$^{-/-}$ cells in the absence of CTB binding and obtained essentially the same results (Figure 6C). However, in the absence of CTB binding, only 20% of the cells at 5 h had detectable GM1 in the ER when loaded with the unsaturated C16:1-GM1 species, as opposed to over 90% when CTB was bound (Figure 6B). Thus, there was a clear effect of crosslinking GM1 caused by toxin binding that increased uptake of GM1 into the cell, or the efficiency of transport in the retrograde pathway, or both.

We also studied MEF GM1$^{-/-}$ cells loaded with GM1 species not labeled with Alexa. Loading conditions for the unlabeled GM1 species was first defined using a horseradish peroxidase (HRP)-labeled CTB binding assay for membrane GM1 content (Figure 6D). Equal loading into the membrane for the GM1-C16:0 and GM1-C16:1 species was confirmed by FACS analysis as described above (Figures S4A – S4C). These studies also showed that the unlabeled GM1 sphingolipids integrated into the PM of MEF GM1$^{-/-}$ cells but with lower efficiency than the Alexa-labeled lipids in A431 cells (about 18% was incorporated into the PM, Figure S4B & S4C), consistent with previous studies using native bovine unlabeled GM1 (Saqr et al., 1993; Scheel et al., 1985). The greater membrane uptake for the Alexa-fluor labeled GM1 lipids may be explained by their additional charge and greater solubility in aqueous solution.

Trafficking of the different unlabeled GM1 species into the ER of the MEF GM1$^{-/-}$ cells was measured using fluorophore-labeled CTB. Consistent with our previous results, we found 6-fold greater efficiency for retrograde sorting of the unsaturated GM1-C16:1 species into the ER (Figure 6E). Similar results were found for the GM1-C12:0 species (data not shown). To confirm that these GM1 variants act as functional receptors for CT leading to toxicity, we measured the time course of toxin-induced cAMP in the MEF-GM1$^{-/-}$ cells loaded equally with the different GM1 species (Figure 6F). Only the short-chain and unsaturated GM1 molecular species with C12:0- and C16:1-ceramides allowed for a rapid and robust toxin-induced cAMP response (Figure 6F). MEF-GM1$^{-/-}$ cells loaded with the C16:0 or C18:0-GM1 variants responded to CT only marginally and with a dramatically slower time-course. Thus, the unsaturated C16:1-GM1 molecular species sorts retrograde from PM to ER by an endogenous lipid-sorting pathway. When bound to CT, it acts as a functional receptor leading to toxicity, and cross-linking C16:1-GM1 by toxin binding does not over-ride the influence of ceramide structure on the sorting process.

We are aware that our analysis of these results is based on the assumption that the exogenous lipids added to A431 cells and mouse embryonic fibroblasts remained structurally intact over the 1–5 h time course for most of our experiments. It was not possible to test this assumption directly: despite multiple attempts, we were unable to recover sufficient quantities of the gangliosides for structural characterization by mass spectroscopy. On the other hand, using thin-layer chromatography we estimated the amounts of the different Alexa-GM1 species extracted from A431 cells by fluorescence and found that between 50–80% of each lipid species loaded into the cell was recovered intact after 4h incubations at 37°C, with no eviden ce for partial degradation of the Alexa-labeled gangliosides (not shown). This indicates that most of the lipid loaded into cells remained intact over the time course of our experiments. Furthermore, there is no evidence for degradation of ganglioside ceramide domains before the oligosaccharide head group is cleaved in the lysosome (Luberto and Hannun, 1999). Thus we consider it unlikely that the ceramides of the added lipids were differentially altered in the early sorting compartments under study here and as further described below.

Mechanism of lipid sorting

How do cells distinguish between the saturated and unsaturated GM1 species, and is the structure of the ceramide domain (molecular shape) sufficient to explain ganglioside trafficking? We first sought evidence for GM1 sorting by lipid-phase behavior, as predicted by the lipid raft hypothesis. A431 cells loaded with the unsaturated GM1-C16:1 isoform and acutely depleted of cholesterol by treatment with methyl-β-cyclodextrin (MβCD) failed to transport this GM1 species from PM into the TGN, either as a single lipid in the absence of crosslinking, or as a CTB-GM1 complex (Figures 7A & 7B). In both cases, the unsaturated GM1-C16:1 species still populated the RE and PM in cholesterol depleted cells (data not shown). Celqlular cholesterol was also required for sorting of the saturated C18:0-GM1 lipids, in this case for trafficking from PM into the LE (Figure 7C). Here, we found that after cholesterol depletion the saturated C18:0-GM1 species was now retained in the RE and PM (Figure 7C, compare left and middle panels); this was reversed by replenishing the cells with cholesterol (Figure 7C, right panel). The fact that cholesterol depletion affected the trafficking of both the saturated and unsaturated GM1 species, retaining them in the plasma membrane and recycling system, suggests that a lipid-raft mechanism is involved in GM1 sorting.

We next tested for dependence on the membrane-associated cortical actin cytoskeleton, which is implicated in lipid raft structure and function. Treatment of A431 cells with cytochalasin D to depolymerize actin inhibited transport of the GM1 C16:1 species from PM into the TGN (Figure 7D). The result suggests dependence on actin for GM1 sorting,

consistent with the observed dependence on actin for trafficking of GPI-anchored proteins by membrane nanodomains (Chadda et al., 2007; Goswami et al., 2008), and with our previous findings that an intact actin cytoskeleton is required for CT uptake and toxicity (Badizadegan et al., 2004).

Finally, we tested for dependence on the lipid raft associated protein flotillin-1. The flotillin proteins are also implicated in lipid raft structure and function, and they are required for CT transport from PM to ER and for toxicity (Saslowsky et al., 2010). We used RNAi from two sources to suppress flotillin in A431 cells loaded with the C16:1-GM1 or C16:0-GM1 sphingolipids (Figures 7E–7K). Flotillin-depleted cells failed to transport the GM1-C16:1 species from the PM into the ER (Figures 7E & 7G, compare first and second columns) or into the TGN (Figure 7I). Flotillin depletion had a small effect on trafficking the C16:1-GM1 lipids in the recycling system (PM and RE, Figure 7J), and no detectable effect on delivery of this species to the LE (Figure 7K). Thus, flotillin appears to be required for sorting the unsaturated GM1-C16:1 lipids, acting particularly at steps leading into the retrograde ER-directed pathway.

DISCUSSION

Our results show that mammalian cells sort single GM1 sphingolipids by ceramide structure and provide insight into the mechanisms of lipid sorting and cholera toxin action. We found that it is the GM1 species with unsaturated ceramide chains that sort efficiently from PM to the TGN and ER. Small amounts of GM1 species with long saturated ceramides also enter the ER in live cells, but very inefficiently and without dependence on flotillin, suggesting a stochastic pathway. This differential sorting of GM1 species may explain the ability of CT to enter host cells by different endocytic pathways and to traffic into multiple intracellular compartments (Glebov et al., 2006; Massol et al., 2004; Parton, 1994; Torgersen et al., 2001), not all of them leading to toxicity.

In contrast to GM1, the extracellular domain, and not the lipid-anchor, dominates trafficking of the GPI-anchored proteins (Bhagatji et al., 2009), although the structure of the glycerol-based lipid anchor has recently been shown to affect sorting into recycling pathways (Refaei et al., 2011). Undoubtedly, the extracellular head group of GM1 and other neighboring lipids will also affect how the single GM1 species behave in membrane dynamics (Lingwood et al., 2010; Sonnino et al., 2007), and ceramide structure will affect toxin binding to the oligosaccharide head group (Arab and Lingwood, 1996; Lingwood et al., 2011). But these aspects of GM1 function were not studied here.

Our results support major tenets of both the “molecular shape” and “lipid raft” hypotheses for lipid sorting, which propose competing but not necessarily exclusive mechanisms. Consistent with the molecular shape model, the unsaturated structure of the ceramide domain in GM1 dictates efficient retrograde trafficking. This does not, however, appear to be fully sufficient to explain GM1 sorting. We find that sorting of the unsaturated GM1 species also depends upon membrane cholesterol and the membrane associated proteins flotillin-1 and actin, consistent with the lipid raft hypothesis for lipid trafficking (Goswami et al., 2008; Jacobson et al., 2007; Kaiser et al., 2009; Lingwood and Simons, 2010; Sorre et al., 2009; Tian and Baumgart, 2009). Compositional fluctuations with different phase-character occur in cell membranes near lipid “demixing” or “miscibility critical points” and though the nanodomains formed may be very small (50 nm) and transient (20 ms half-life) (Eggeling et al., 2009; Heinrich et al., 2010; Honerkamp-Smith et al., 2009; Lingwood et al., 2008; Sorre et al., 2009; Tian et al., 2009), there is good evidence they are biologically active (Lingwood et al., 2010) and that the CT-GM1 complex can associate with them (Baumgart et al., 2007; Lingwood et al., 2008).

Remarkably, the unsaturated GM1 sphingolipids that sort retrograde to the ER in live cells partition predominantly into L_d phases of GUVs when cross-linked by CTB. This behavior in GUVs does not typify the lipids predicted to associate with lipid rafts and suggests that the way membrane lipids assemble into nanodomains of live cells may be more diverse than currently hypothesized. Perhaps in live cell membranes with complex lipid and protein compositions, lipid rafts can be structured to accommodate the unsaturated GM1 species, either by direct or indirect protein-lipid binding. Flotillin could be one such protein. It is also interesting to consider that the unsaturated GM1 species may allow for dynamic phase segregations in membranes with miscibility critical points that change during the process of vesicular trafficking (a feature perhaps unavailable to the saturated GM1 lipids). Our results in cholesterol-depleted cells suggest such phase segregations may occur in the sorting endosome.

We also note that CT will likely bind multiple GM1 species in the same cell membrane, unless the toxin can discriminate between GM1 with different ceramides as for Shiga toxin binding *in vitro* to the globoside Gb3 (Arab and Lingwood, 1996). Our results, however, predict that CT binding to mostly long saturated GM1 ceramides would inhibit retrograde trafficking and render the cell resistant to intoxication.

The identification of the GM1 species with unsaturated ceramides as physiologic receptors for trafficking CT was not fully expected, as the closely related Shiga toxin and the SV40 virus require binding to glycosphingolipids with long saturated ceramide domains to travel from PM to ER and induce toxicity (Ewers et al., 2010; Raa et al., 2009; Sandvig et al., 1994). Unlike CT, however, Shiga toxin and SV40 virus have the potential to scaffold a greater number of glycosphingolipid receptors together (360 GM1 and 15 Gb3 molecules respectively) (Ewers et al., 2010; Johannes and Mayor, 2010; Romer et al., 2007; Romer et al., 2010), and this could induce distinct mechanisms of lipid sorting unavailable to CT. A recent study shows that retrograde sorting depends critically on Shiga toxin binding not only to glycosphingolipid, but also to the endosomal membrane protein GPP130 (Mukhopadhyay and Linstedt, 2012). Perhaps once in the TGN, the long saturated ceramide domain of the toxin's receptor Gb3 facilitates this interaction. No such dependence on GPP130 was found for CT (Mukhopadhyay and Linstedt, 2012).

On the other hand, there is evidence from studies on Shiga toxin (Romer et al., 2007) that anticipate sorting by glycosphingolipid receptors with unsaturated ceramide domains. Upon binding to the unsaturated species of Gb3 in model membranes, Shiga toxin spontaneously induces highly curved tubules (Romer et al., 2007). CT binding to GM1 in model membranes also induces spontaneous membrane curvature and tubule formation (Heinrich et al., 2010; Sorre et al., 2009; Tian et al., 2009). Thus, aside from any effect on phase partitioning, the spontaneous curvature induced by toxin binding to GM1, perhaps amplified by binding to the unsaturated GM1 species (as for Shiga toxin binding Gb3), may *in vivo* allow for partitioning of the CT-GM1 complex into sorting tubules required for retrograde transport. This could account for the increased ER transport of GM1 induced by toxin binding. Toxin binding to the unsaturated GM1 species may also activate intracellular signaling pathways that enhance uptake and trafficking, as for Shiga toxin (Torgersen et al., 2001). Either mechanism of action could underlie how the CTB-subunit, and the other AB_5 toxins, evolved as essentially pentameric structures.

Our findings, we believe, can be generalized to explain the pathogenesis of disease induced by *V. cholerae,* as intestinal cells express a number of different GM1 species with ceramide acyl chains of C24:0, C24:1, C16:0, and C16:1 predominating (Lencer and Costello, unpublished data). In this study, we focused on the C16:1 and C16:0 variants, but our results

show the C18:1 molecular species behave in the same way, suggesting a general rule for sphingolipid transport in the retrograde pathways.

Based on our results, we propose the following model for GM1 sorting (see Graphic Abstract). In the absence of CT, the GM1 species with unsaturated ceramides continuously recycle between the PM and early SE and RE with a fraction constitutively captured by actin-, flotillin-, and cholesterol-dependent nanodomains for retrograde transport to the TGN and ER. The long chain saturated GM1 isoforms also enter the early SE but are efficiently sorted to the LE. Thus, CT co-opts an endogenous unsaturated-sphingolipid and flotilin-dependent pathway to intoxicate host cells. While crosslinking GM1 by toxin binding enhances retrograde transport (Wolf et al., 2008), it is not required. Surprisingly, the major effect of CT binding on GM1 trafficking is to cluster the recycling GM1 species, driving most of them into the degradative LE and lysosome.

METHODS

List of Materials is in the Supplemental Experimental Procedures.

Imaging and Quantitative analysis of GUVs

GUVs were prepared and imaged as previously described (Tian et al., 2009). The phase partition for GM1-CTB-A488 complex in GUVs (Figure 1C) was determined by quantitative image analysis through ImageJ (National Institute of Health, Bethesda, MD). Further details in Supplemental Experimental Procedures.

FRAP Measurements

A431 cells were plated on coverslips or MatTek chambers and fluorophore-labeled GM1 isoforms were added at 0.5–2.0 μM concentrations at 10°C to load the plasma membranes. Alternatively, cells were incubated for 5 minutes at room temperature with 100 nM of Alexa555-CTxB or 2.5 μg/ml $DiIC_{16}$ (both obtained from Invitrogen, Carlsbad, CA). Cells were then washed and confocal FRAP experiments were carried out on a Zeiss LSM 510 confocal microscope (Carl Zeiss MicroImaging, Inc., Thornwood, NY) at 37° C as described in the Supplementary materials. FRAP data were collected for at least three independent experiments.

Cell Culture and siRNA Knockdown

Human epithelial A431 cells were from the American Tissue Culture Collection (ATCC, VA). Mouse embryonic fibroblasts (MEFs) lacking GM1 ganglioside were generated from mouse cell lines genetically knocked out for the GM2/GD2 synthase gene. Cells were grown and maintained in Dulbecco's Modified Eagle's Medium (DMEM) containing 10% FBS with penicillin and streptomycin. Stable A431 cell lines expressing EGFP fusion constructs for Rab5, Rab7, Rab11 and Golgin97 were generated by transfection with Lipofectamine2000 reagent (Life Technologies, CA) followed by selection in G418 antibiotic and single-cell cloning. For siRNA knockdown in A431 cells, siRNAs against syntaxin6, rab9 (Life Technologies, CA) and flotillin-1 (Santa Cruz, CA or Thermo, CO) were transfected into cells plated on coverslips and used for experiments 48–72 hours later. See Supplemental Experimental Procedures.

Synthesis of GM1 Fatty Acyl and Fluorophore-Labeled Isoforms

Synthesis and labeling of GM1 containing different fatty acids is described in Supplemental Experimental Procedures.

Live Cell Imaging

Stable A431 cells were plated on coverslips and fluorophore-labeled GM1 isoforms were added at 0.5–2.0 μM concentrations at 10°C to load the plasma membranes. Cells were allowed to warm up to 37°C to allow for endocytosis and reach steady-state. 40 nM CTB (Merck, Germany) in HBSS was added in some experiments prior to warming for 90 minutes. Cells were imaged live using a Zeiss Spinning Disk Confocal microscope and data captured and analyzed with Slidebook software (Intelligent Imaging Innovations, CO). Colocalization to EGFP-labeled endosomes/organelles was quantified using Manders and Pearson's Coefficients (M_x and Rr respectively) as detailed in Supplemental Experimental Procedures. In all cases, except for analysis of GM1 distribution among endosomes in the absence of CTB binding (Figure 2A), the M_x and Rr results are internally consistent.

Normalization of GM1 Plasma Membrane Loading

MEF-GM1$^{-/-}$ cells were plated in 96-well plates and incubated with varying concentrations of GM1 isoforms to label the plasma membrane at 10 °C. Horse radish peroxidase-conjugated CTB (20 nM) was then added to bind GM1 loaded on cells. Cell membranes were lysed in detergent-containing buffer and the peroxidase signal in the lysates was measured using a colorimetric method. See Supplemental Experimental Procedures for details.

Cholesterol Depletion Studies

A431 cells were plated onto coverslips in 6-well plates and treated with 5 mM MβCD in HBSS for 1 hour at 37 °C to acutely deplete of membranes of cholesterol. Cells were washed then chilled to 10 °C followed by loading with fluorescent GM1 isoforms in HBSS for 30 minutes. Cells were either not treated, or treated with 40 nM CTB at 37 °C for 90 minutes then imaged by confocal microscopy as explained above.

Actin Depolymerization Studies

A431 cells plated as above were pre-treated with 20 μM cytochalasin D in Opti-MEM for 30 minutes. Cells were then chilled to 10 °C and Alexa GM1 complexes in HBSS containing 20 μM cytochalasin D were added to load the membranes for 1 hour. After washing, cells were warmed up to 37 °C in Opti-MEM containing cytochalasin D and imaged after 75 – 90 minutes by confocal microscopy.

Measurement of Intracellular cAMP Levels

Intracellular cAMP in MEF-GM1$^{-/-}$ cells treated with CT for 15, 30, 45, or 60 minutes was measured using an EIA cAMP kit (GE Biosciences, NJ) as described previously (Saslowsky et al., 2010).

Supplementary Material

Refer to Web version on PubMed Central for supplementary material.

Acknowledgments

We thank Tomas Kirchhausen for plasmids containing EGFP-fusions to Rab5, Rab11a, Golgin97, and Sec61α, Susanne Pfeffer for the gift of Rab9 antibodies; Marian Neutra for critical reading of the manuscript; the entire Lencer lab group for helpful discussions; Wendy Kam for tissue culture; and Marc-Andre Wurbel for help with flow cytometry. This study was funded by NIH grants R01 DK48106, R01 DK084424, and R21 DK090603 (to W.I.L.); NSERC Canada PDF (to D.J.C); K01 DK073480 and R03 DK084090 (to D.E.S); RO1 CA 082395 (to T. Benjamin), R21 AI073409, NSF MCB-0718569 and an A.P. Sloan Fellowship (to T. Baumgart); P41 RR10888 (to C.E.C), RO1 GM073846 and NSF/DMS 0970008 (to A.K.) and the Harvard Digestive Diseases Center P30 DK34854.

References

Arab S, Lingwood CA. Influence of phospholipid chain length on verotoxin/globotriaosyl ceramide binding in model membranes: comparison of a supported b film and liposomes. Glycoconj J. 1996; 13:159–166. [PubMed: 8737240]

Badizadegan K, Wheeler HE, Fujinaga Y, Lencer WI. Trafficking of cholera toxin-ganglioside GM1 complex into Golgi and induction of toxicity depend on actin cytoskeleton. Am J Physiol Cell Physiol. 2004; 287:C1453–1462. [PubMed: 15294854]

Baumgart T, Hammond AT, Sengupta P, Hess ST, Holowka DA, Baird BA, Webb WW. Large-scale fluid/fluid phase separation of proteins and lipids in giant plasma membrane vesicles. Proc Natl Acad Sci U S A. 2007; 104:3165–3170. [PubMed: 17360623]

Bhagatji P, Leventis R, Comeau J, Refaei M, Silvius JR. Steric and not structure-specific factors dictate the endocytic mechanism of glycosylphosphatidylinositol-anchored proteins. J Cell Biol. 2009; 186:615–628. [PubMed: 19687251]

Brown FL, Leitner DM, McCammon JA, Wilson KR. Lateral diffusion of membrane proteins in the presence of static and dynamic corrals: suggestions for appropriate observables. Biophys J. 2000; 78:2257–2269. [PubMed: 10777724]

Brown RE, Mattjus P. Glycolipid transfer proteins. Biochim Biophys Acta. 2007; 1771:746–760. [PubMed: 17320476]

Cantu L, Del Favero E, Sonnino S, Prinetti A. Gangliosides and the multiscale modulation of membrane structure. Chem Phys Lipids. 2011; 164:796–810. [PubMed: 21946022]

Chadda R, Howes MT, Plowman SJ, Hancock JF, Parton RG, Mayor S. Cholesterol-sensitive Cdc42 activation regulates actin polymerization for endocytosis via the GEEC pathway. Traffic. 2007; 8:702–717. [PubMed: 17461795]

Cuatrecasas P. Gangliosides and membrane receptors for cholera toxin. Biochemistry. 1973; 12:3558–3566. [PubMed: 4731192]

Eggeling C, Ringemann C, Medda R, Schwarzmann G, Sandhoff K, Polyakova S, Belov VN, Hein B, von Middendorff C, Schonle A, et al. Direct observation of the nanoscale dynamics of membrane lipids in a living cell. Nature. 2009; 457:1159–1162. [PubMed: 19098897]

Ewers H, Romer W, Smith AE, Bacia K, Dmitrieff S, Chai W, Mancini R, Kartenbeck J, Chambon V, Berland L, et al. GM1 structure determines SV40-induced membrane invagination and infection. Nat Cell Biol. 2010; 12:11–18. sup pp 11–12. [PubMed: 20023649]

Falguieres T, Mallard F, Baron C, Hanau D, Lingwood C, Goud B, Salamero J, Johannes L. Targeting of Shiga toxin B-subunit to retrograde transport route in association with detergent-resistant membranes. Mol Biol Cell. 2001; 12:2453–2468. [PubMed: 11514628]

Fujinaga Y, Wolf AA, Rodighiero C, Wheeler H, Tsai B, Allen L, Jobling MG, Rapoport T, Holmes RK, Lencer WI. Gangliosides that associate with lipid rafts mediate transport of cholera and related toxins from the plasma membrane to endoplasmic reticulm. Mol Biol Cell. 2003; 14:4783–4793. [PubMed: 13679513]

Ganley IG, Espinosa E, Pfeffer SR. A syntaxin 10-SNARE complex distinguishes two distinct transport routes from endosomes to the trans-Golgi in human cells. J Cell Biol. 2008; 180:159–172. [PubMed: 18195106]

Glebov OO, Bright NA, Nichols BJ. Flotillin-1 defines a clathrin-independent endocytic pathway in mammalian cells. Nat Cell Biol. 2006; 8:46–54. [PubMed: 16341206]

Goswami D, Gowrishankar K, Bilgrami S, Ghosh S, Raghupathy R, Chadda R, Vishwakarma R, Rao M, Mayor S. Nanoclusters of GPI-anchored proteins are formed by cortical actin-driven activity. Cell. 2008; 135:1085–1097. [PubMed: 19070578]

Gupta VR, Wilson BA, Blanke SR. Sphingomyelin is important for the cellular entry and intracellular localization of Helicobacter pylori VacA. Cell Microbiol. 2010; 12:1517–1533. [PubMed: 20545942]

Hakomori S. Structure, organization, and function of glycosphingolipids in membrane. Curr Opin Hematol. 2003; 10:16–24. [PubMed: 12483107]

Hammond AT, Heberle FA, Baumgart T, Holowka D, Baird B, Feigenson GW. Crosslinking a lipid raft component triggers liquid ordered-liquid disordered phase separation in model plasma membranes. Proc Natl Acad Sci U S A. 2005; 102:6320–6325. [PubMed: 15851688]

Heinrich M, Tian A, Esposito C, Baumgart T. Dynamic sorting of lipids and proteins in membrane tubes with a moving phase boundary. Proc Natl Acad Sci U S A. 2010; 107:7208–7213. [PubMed: 20368457]

Honerkamp-Smith AR, Veatch SL, Keller SL. An introduction to critical points for biophysicists; observations of compositional heterogeneity in lipid membranes. Biochim Biophys Acta. 2009; 1788:53–63. [PubMed: 18930706]

Jacobson K, Mouritsen OG, Anderson RG. Lipid rafts: at a crossroad between cell biology and physics. Nat Cell Biol. 2007; 9:7–14. [PubMed: 17199125]

Johannes L, Mayor S. Induced domain formation in endocytic invagination, lipid sorting, and scission. Cell. 2010; 142:507–510. [PubMed: 20723749]

Johannes L, Popoff V. Tracing the retrograde route in protein trafficking. Cell. 2008; 135:1175–1187. [PubMed: 19109890]

Johnson SA, Stinson BM, Go MS, Carmona LM, Reminick JI, Fang X, Baumgart T. Temperature-dependent phase behavior and protein partitioning in giant plasma membrane vesicles. Biochim Biophys Acta. 2010; 1798:1427–1435. [PubMed: 20230780]

Kaiser HJ, Lingwood D, Levental I, Sampaio JL, Kalvodova L, Rajendran L, Simons K. Order of lipid phases in model and plasma membranes. Proc Natl Acad Sci U S A. 2009; 106:16645–16650. [PubMed: 19805351]

Kenworthy AK, Nichols BJ, Remmert CL, Hendrix GM, Kumar M, Zimmerberg J, Lippincott-Schwartz J. Dynamics of putative raft-associated proteins at the cell surface. J Cell Biol. 2004; 165:735–746. [PubMed: 15173190]

Koivusalo M, Jansen M, Somerharju P, Ikonen E. Endocytic trafficking of sphingomyelin depends on its acyl chain length. Mol Biol Cell. 2007; 18:5113–5123. [PubMed: 17942604]

Lencer WI, Tsai B. The intracellular voyage of cholera toxin: going retro. Trends Biochem Sci. 2003; 28:639–645. [PubMed: 14659695]

Lingwood CA, Manis A, Mahfoud R, Khan F, Binnington B, Mylvaganam M. New aspects of the regulation of glycosphingolipid receptor function. Chem Phys Lipids. 2010; 163:27–35. [PubMed: 19781539]

Lingwood D, Binnington B, Rog T, Vattulainen I, Grzybek M, Coskun U, Lingwood CA, Simons K. Cholesterol modulates glycolipid conformation and receptor activity. Nat Chem Biol. 2011; 7:260–262. [PubMed: 21460830]

Lingwood D, Kaiser HJ, Levental I, Simons K. Lipid rafts as functional heterogeneity in cell membranes. Biochem Soc Trans. 2009; 37:955–960. [PubMed: 19754431]

Lingwood D, Ries J, Schwille P, Simons K. Plasma membranes are poised for activation of raft phase coalescence at physiological temperature. Proc Natl Acad Sci U S A. 2008; 105:10005–10010. [PubMed: 18621689]

Lingwood D, Simons K. Lipid rafts as a membrane-organizing principle. Science. 2010; 327:46–50. [PubMed: 20044567]

Luberto C, Hannun YA. Sphingolipid metabolism in the regulation of bioactive molecules. Lipids. 1999; 34(Suppl):S5–11. [PubMed: 10419081]

Mallard F, Antony C, Tenza D, Salamero J, Goud B, Johannes L. Direct pathway from early/recycling endosomes to the Golgi apparatus revealed through the study of shiga toxin B-fragment transport. J Cell Biol. 1998; 143:973–990. [PubMed: 9817755]

Masserini M, Palestini P, Pitto M, Chigorno V, Tomasi M, Tettamanti G. Cyclic AMP accumulation in HeLa cells induced by cholera toxin. Involvement of the ceramide moiety of GM1 ganglioside. Biochem J. 1990; 271:107–111. [PubMed: 2171494]

Massol RH, Larsen JE, Fujinaga Y, Lencer WI, Kirchhausen T. Cholera toxin toxicity does not require functional Arf6- and dynamin-dependent endocytic pathways. Mol Biol Cell. 2004; 15:3631–3641. [PubMed: 15146065]

Mukherjee S, Soe TT, Maxfield FR. Endocytic sorting of lipid analogues differing solely in the chemistry of their hydrophobic tails. J Cell Biol. 1999; 144:1271–1284. [PubMed: 10087269]

Mukhopadhyay S, Linstedt AD. Manganese blocks intracellular trafficking of Shiga toxin and protects against Shiga toxicosis. Science. 2012; 335:332–335. [PubMed: 22267811]

Neumann S, van Meer G. Sphingolipid management by an orchestra of lipid transfer proteins. Biol Chem. 2008; 389:1349–1360. [PubMed: 18783332]

Nilsson O, Svennerholm L. Characterization and quantitative determination of gangliosides and neutral glycosphingolipids in human liver. J Lipid Res. 1982; 23:327–334. [PubMed: 7077147]

Orlandi PA, Fishman PH. Filipin-dependent inhibition of cholera toxin: evidence for toxin internalization and activation through caveolae-like domains. J Cell Biol. 1998; 141:905–915. [PubMed: 9585410]

Panasiewicz M, Domek H, Hoser G, Kawalec M, Pacuszka T. Structure of the ceramide moiety of GM1 ganglioside determines its occurrence in different detergent-resistant membrane domains in HL-60 cells. Biochemistry. 2003; 42:6608–6619. [PubMed: 12767245]

Parton RG. Ultrastructural localization of gangliosides; GM1 is concentrated in caveolae. J Histochem Cytochem. 1994; 42:155–166. [PubMed: 8288861]

Raa H, Grimmer S, Schwudke D, Bergan J, Walchli S, Skotland T, Shevchenko A, Sandvig K. Glycosphingolipid requirements for endosome-to-Golgi transport of Shiga toxin. Traffic. 2009; 10:868–882. [PubMed: 19453975]

Refaei M, Leventis R, Silvius JR. Assessment of the roles of ordered lipid microdomains in post-endocytic trafficking of glycosyl-phosphatidylinositol-anchored proteins in mammalian fibroblasts. Traffic. 2011; 12:1012–1024. [PubMed: 21696526]

Romer W, Berland L, Chambon V, Gaus K, Windschiegl B, Tenza D, Aly MR, Fraisier V, Florent JC, Perrais D, et al. Shiga toxin induces tubular membrane invaginations for its uptake into cells. Nature. 2007; 450:670–675. [PubMed: 18046403]

Romer W, Pontani LL, Sorre B, Rentero C, Berland L, Chambon V, Lamaze C, Bassereau P, Sykes C, Gaus K, et al. Actin dynamics drive membrane reorganization and scission in clathrin-independent endocytosis. Cell. 2010; 140:540–553. [PubMed: 20178746]

Safouane M, Berland L, Callan-Jones A, Sorre B, Romer W, Johannes L, Toombes GE, Bassereau P. Lipid cosorting mediated by shiga toxin induced tubulation. Traffic. 2010; 11:1519–1529. [PubMed: 20887377]

Sandvig K, Dubinina E, Garred O, Prydz K, Kozlov JV, Hansen SH, van Deurs B. Protein toxins: mode of action and cell entry. Biochem Soc Trans. 1992; 20:724–727. [PubMed: 1487049]

Sandvig K, Ryd M, Garred O, Schweda E, Holm PK, van Deurs B. Retrograde transport from the Golgi complex to the ER of both Shiga toxin and the nontoxic Shiga B-fragment is regulated by butyric acid and cAMP. J Cell Biol. 1994; 126:53–64. [PubMed: 8027186]

Saqr HE, Pearl DK, Yates AJ. A review and predictive models of ganglioside uptake by biological membranes. J Neurochem. 1993; 61:395–411. [PubMed: 8336130]

Saslowsky DE, Cho JA, Chinnapen H, Massol RH, Chinnapen DJ, Wagner JS, De Luca HE, Kam W, Paw BH, Lencer WI. Intoxication of zebrafish and mammalian cells by cholera toxin depends on the flotillin/reggie proteins but not Derlin-1 or -2. J Clin Invest. 2010; 120:4399–4409. [PubMed: 21041954]

Scheel G, Schwarzmann G, Hoffmann-Bleihauer P, Sandhoff K. The influence of ganglioside insertion into brain membranes on the rate of ganglioside degradation by membrane-bound sialidase. Eur J Biochem. 1985; 153:29–35. [PubMed: 2998792]

Schwarzmann G. Uptake and metabolism of exogenous glycosphingolipids by cultured cells. Semin Cell Dev Biol. 2001; 12:163–171. [PubMed: 11292382]

Sharma P, Varma R, Sarasij RC, Ira, Gousset K, Krishnamoorthy G, Rao M, Mayor S. Nanoscale organization of multiple GPI-anchored proteins in living cell membranes. Cell. 2004; 116:577–589. [PubMed: 14980224]

Simons K, Gerl MJ. Revitalizing membrane rafts: new tools and insights. Nat Rev Mol Cell Biol. 2010; 11:688–699. [PubMed: 20861879]

Smith DC, Sillence DJ, Falguieres T, Jarvis RM, Johannes L, Lord JM, Platt FM, Roberts LM. The association of Shiga-like toxin with detergent-resistant membranes is modulated by glucosylceramide and is an essential requirement in the endoplasmic reticulum for a cytotoxic effect. Mol Biol Cell. 2006; 17:1375–1387. [PubMed: 16381816]

Sonnino S, Mauri L, Chigorno V, Prinetti A. Gangliosides as components of lipid membrane domains. Glycobiology. 2007; 17:1R–13R.

Sorre B, Callan-Jones A, Manneville JB, Nassoy P, Joanny JF, Prost J, Goud B, Bassereau P. Curvature-driven lipid sorting needs proximity to a demixing point and is aided by proteins. Proc Natl Acad Sci U S A. 2009; 106:5622–5626. [PubMed: 19304798]

Spooner RA, Lord JM. How ricin and Shiga toxin reach the cytosol of target cells: retrotranslocation from the endoplasmic reticulum. Curr Top Microbiol Immunol. 2012; 357:19–40. [PubMed: 21761287]

Tian A, Baumgart T. Sorting of lipids and proteins in membrane curvature gradients. Biophys J. 2009; 96:2676–2688. [PubMed: 19348750]

Tian A, Capraro BR, Esposito C, Baumgart T. Bending stiffness depends on curvature of ternary lipid mixture tubular membranes. Biophys J. 2009; 97:1636–1646. [PubMed: 19751668]

Torgersen ML, Skretting G, van Deurs B, Sandvig K. Internalization of cholera toxin by different endocytic mechanisms. J Cell Sci. 2001; 114:3737–3747. [PubMed: 11707525]

Tzaban S, Massol RH, Yen E, Hamman W, Frank SR, Lapierre LA, Hansen SH, Goldenring JR, Blumberg RS, Lencer WI. The recycling and transcytotic pathways for IgG transport by FcRn are distinct and display an inherent polarity. J Cell Biol. 2009; 185:673–684. [PubMed: 19451275]

Veatch SL, Keller SL. Separation of liquid phases in giant vesicles of ternary mixtures of phospholipids and cholesterol. Biophys J. 2003; 85:3074–3083. [PubMed: 14581208]

Wolf AA, Jobling MG, Saslowsky DE, Kern E, Drake KR, Kenworthy AK, Holmes RK, Lencer WI. Attenuated endocytosis and toxicity of a mutant cholera toxin with decreased ability to cluster ganglioside GM1 molecules. Infect Immun. 2008; 76:1476–1484. [PubMed: 18212085]

Wolf AA, Jobling MG, Wimer-Mackin S, Ferguson-Maltzman M, Madara JL, Holmes RK, Lencer WI. Ganglioside structure dictates signal transduction by cholera toxin and association with caveolae-like membrane domains in polarized epithelia. J Cell Biol. 1998; 141:917–927. [PubMed: 9585411]

Yamashita H, Kubushiro K, Ma J, Fujii T, Tsukazaki K, Iwamori M, Nozawa S. Alteration in the metastatic potential of ovarian cancer cells by transfection of the antisense gene of beta-1,4-galactosyltransferase. Oncol Rep. 2003; 10:1857–1862. [PubMed: 14534708]

HIGHLIGHTS

- Cells sort the glycosphingolipid GM1 by the structure of its ceramide domain (76/89)
- Only unsaturated GM1 ceramides sort retrograde all the way to the ER (64/78)
- GM1 is the vehicle that carries cholera toxin from plasma membrane to ER (61/74)
- Flotillin, cholesterol, and actin are required for GM1 sorting (55/64)

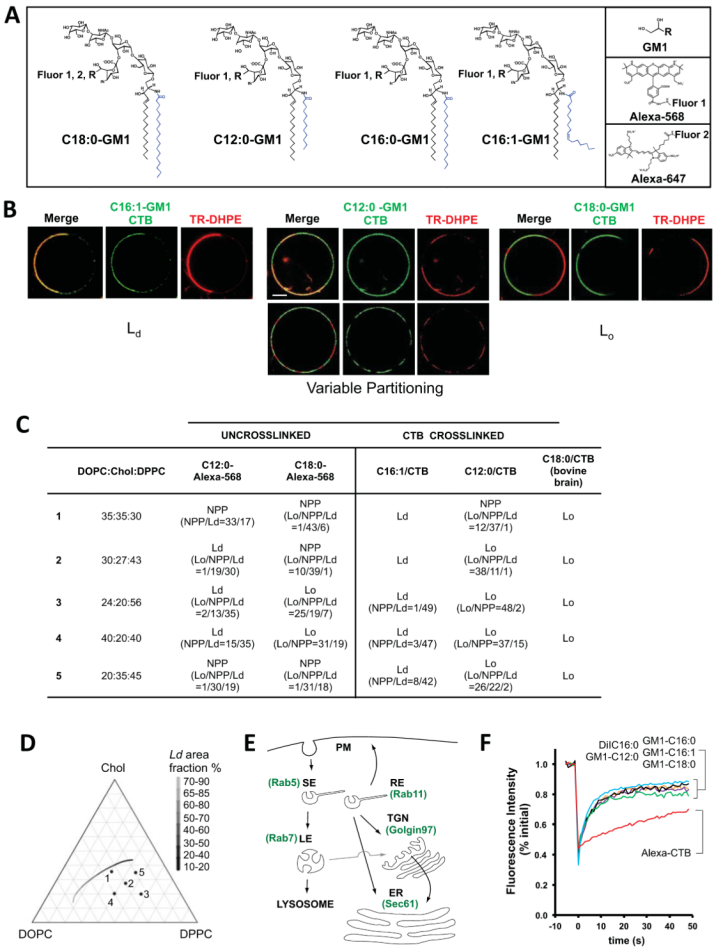

Figure 1. GM1 with different ceramide domains partition into L_o or L_d regions of artificial membranes

A: Structures of GM1 synthesized, Alexa Fluors used and site of conjugation to sialic acid. See also Supplemental Figure S1 and Table S1.

B: Confocal equatorial images of GUVs with DOPC:Chol:DPPC compositions 1 or 3 (Panel c) show different phase partitioning of GM1-CTB complexes, TR-DHPE (red, marking L_d) and GM1-CTB-Alexa488 (green). Left GUV-composition-1: CTB-C16:1 GM1 complex shows L_d phase preference. Middle (top) GUV-composition-1: CTB-C12:0 GM1 complex shows variable phase partitioning. Middle (bottom) GUV-composition-3: CTB-C12:0 GM1 complex shows L_o phase preference. Right GUV-composition-1: CTB-C18:0 GM1 complex shows L_o phase preference. Bar = 10 μm.

C: Phase partitioning of Alexa-labeled GM1 and crosslinked GM1-CTB-A488 complexes in GUVs of different lipid cholesterol compositions. When variable, the ratios for the number of vesicles with the observed phases are shown in the parentheses.

D: Partial ternary phase diagram showing the five GUV lipid-compositions used in these studies. The gray scale line shows the approximate position of a phase coexistence boundary (Tian et al., 2009; Veatch and Keller, 2003) and referencing the domain area fraction of the L_d phase, which decreases with increasing DPPC content (Tian et al., 2009).

E: Schematic of endocytic and retrograde pathways and EGFP-fusion proteins used to mark the indicated compartments.

F: Confocal FRAP of the different Alexa-labeled GM1 species introduced into A431 cells. All GM1 variants (containing fatty acids: C12:0 – orange line, C16:0 – purple line, C16:1 –

black line, C18:0 green-line) displayed D values of approximately 1.3 um^2/s nearly equal to that of an established lipid probe, $DiIC_{16}$ (~1.87um^2/s, blue line). Alexa-555 CTB (red line) diffused substantially slower (D ~ 0.08 um^2/s).
See also Figure S1.

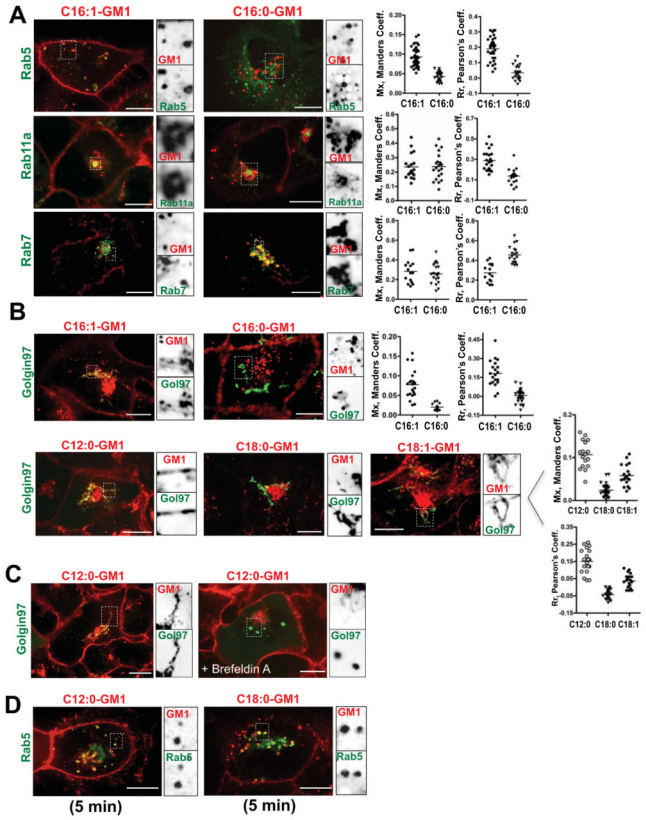

Figure 2. Intracellular distribution of the different GM1 species

A,B: Confocal images of live A431 cells stably expressing EGFP fusion proteins as indicated (Figure 1E). Cells were imaged 50–60 minutes after loading with Alexa-labeled 1.6 μM C16:1- or 2.0 μM C16:0- GM1 molecular species (A), and 1.0 μM C12:0, 2.0 μM C18:0 and C18:1 Alexa-GM1 variants (B). Inverted grayscale images of selected areas (dotted box) for individual fluorescence channels are shown to the right of the merged images. Histograms (far right) show quantitation of GM1 localized to the respective compartment using Manders (M_x), or Pearson's (Rr) coefficients for at least 3 independent experiments. Each dot represents a correlation coefficient calculated from a single field of view containing 2 – 3 cells on average. Overall brightness of the red channels in (B) images was enhanced to better visualize TGN signals.

C: As for panels (A) and (B) using Golgin97-EGFP expressing cells pretreated, or not with 10 μM Brefeldin A followed by uptake for 60 minutes of Alexa-labeled C12:0-GM1. Fraction of lipid signal in the TGN were $M_x = 0.088$ for untreated versus $M_x = 0.007$ for Brefeldin A –treated cells. N = 26 cells analyzed per treatment.

D: As for panels (A) and (B) using cells loaded with short chain (C12:0) or long chain (C18:0) Alexa-GM1 and imaged after 5 minutes uptake. The fraction of total lipid in the Rab5 compartment at this time point were 0.07 for C12:0-GM1 and 0.11 for C18:0-GM1. N = 45 cells analyzed per treatment. Scale bars = 10 μm.

See also Figure S2.

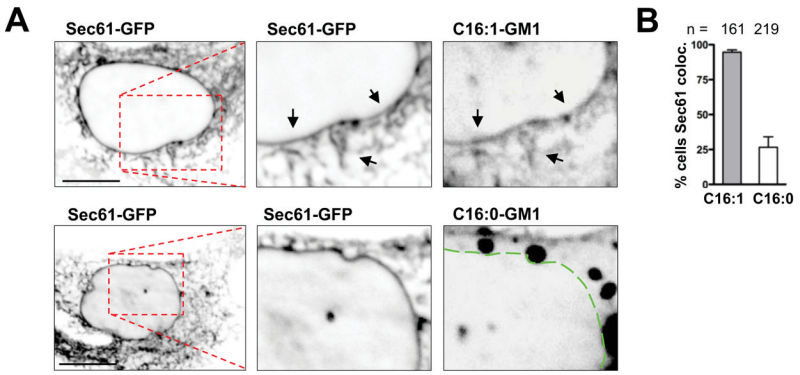

Figure 3. GM1 isoforms with unsaturated acyl chains move efficiently from PM to ER

A: Confocal images of live A431 cells expressing Sec61-EGFP and incubated 18 hours with Alexa568-labeled C16:0- or C16:1-GM1 isoforms. Arrows and dotted line indicate nuclear envelope/ER.

B: Quantification of three independent experiments shown in panel A. (mean ± SEM)

See also Figure S3.

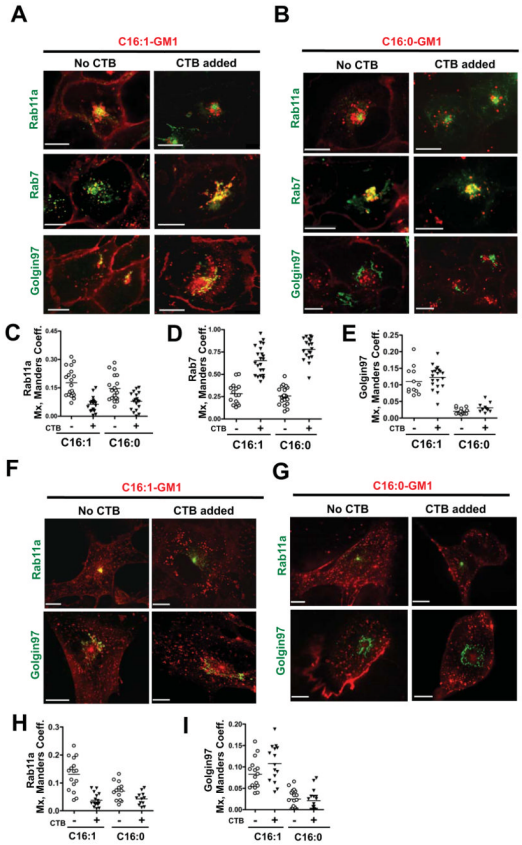

Figure 4. Effect of crosslinking GM1 by binding to CTB

A: A431 cells loaded with C16:1-GM1 and incubated with or without 40 nM CTB (Right and Left panels respectively). Scale bars = 10 μm.

B: Same as in panel (A) using A431 cells loaded with Alexa C16:0-GM1.

C–E: Histograms quantitating the colocalization (M_x) of the C16:1- and C16:0-GM1 molecular species with Rab11a, Rab7 and Golgin97 compartments in cells treated with CTB (filled triangles) or with no toxin (open circles).

F: C16:1-GM1 Alexa568 loaded MEF-GM1$^{-/-}$ cells transiently expressing Rab11a (upper panels) and Golgin97-EGFP (lower panels) treated with 40 nM CTB or without toxin.

G: C16:0-GM1 loaded MEF-GM1$^{-/-}$ cells and treated as in (F).

H and I: Histograms quantitating the colocalization of the C16:1- and C16:0-GM1 isoforms with Rab11a and Golgin97 compartments as indicated. Open circles (no toxin) and filled triangles (plus CTB) as in Panels (C & D). N = 2 independent experiments. Scale bars = 10 μm.

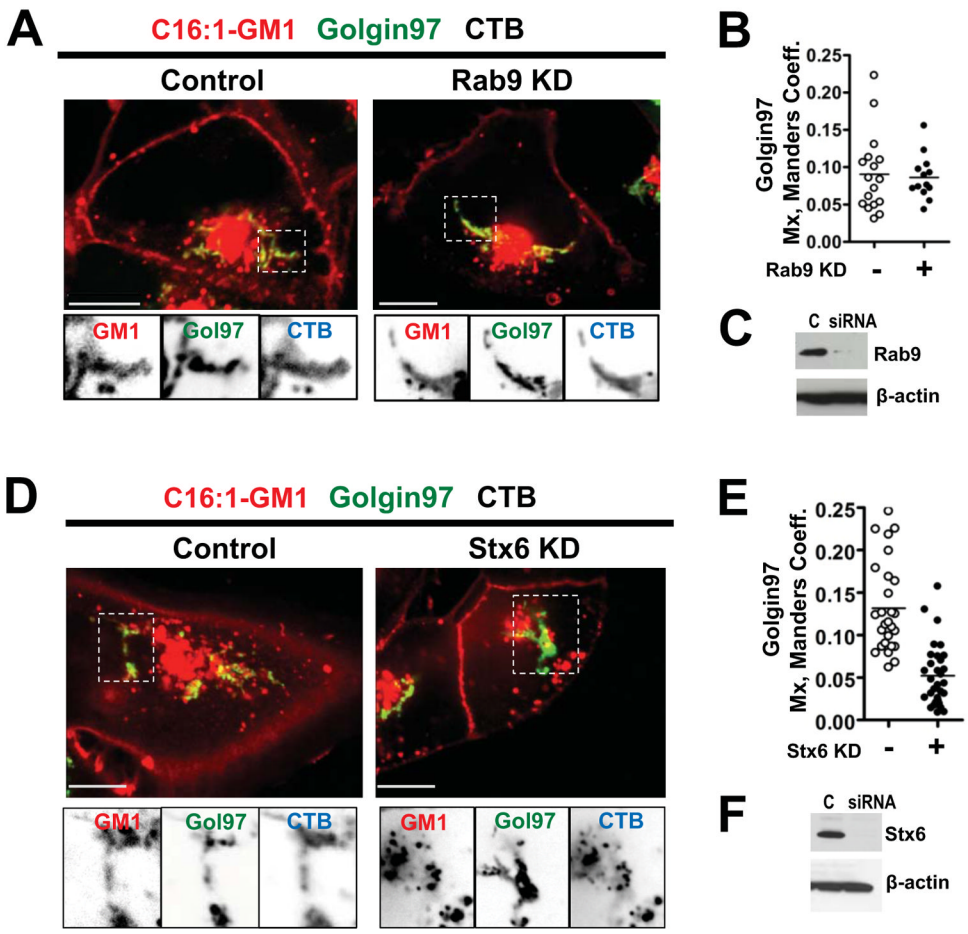

Figure 5. The CT-GM1 complex moves from the SE/RE directly to the TGN

A: A431 cells expressing Golgin97-EGFP and transfected with Rab9 siRNA (right), or controls (left), before incubations with Alexa-labeled C16:1-GM1 and CTB. Inverted grayscale images of selected areas (dotted box) for each channel shown below.

B: Histograms quantitating the colocalization of the Alexa GM1-C16:1 complex with Golgin97 in cells transfected with Rab9 siRNA (closed circles), or in controls (open circles).

C: Immunoblots of cell lysates probed with mouse anti-Rab9 antibody (upper panel) or with mouse anti-β-actin (lower panel).

D: A431 cells transfected with Stx6 siRNA (right), or controls (left) and treated as in (A).

E: Histograms quantitating the colocalization of Alexa C16:1 GM1 with Golgin97 in cells transfected with syntaxin6 (Stx6) siRNA as in (D).

F: Immunoblots probed with mouse anti-Stx6 antibody (upper panel) or with mouse anti-β-actin (lower panel).

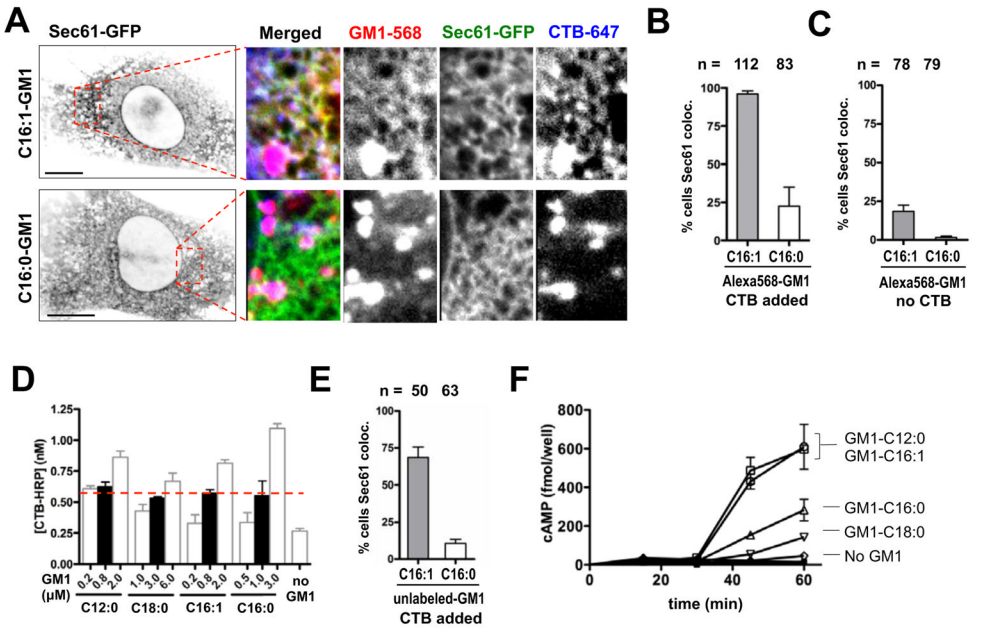

Figure 6. Crosslinked unsaturated acyl chains traffic retrograde more efficiently to the ER

A: Confocal images of Alexa-labeled C16-GM1 isoforms (3.2 μM C16:1-GM1, or 4.0 μM C16:0-GM1) in MEF-GM1$^{-/-}$ cells after 5 hour incubation with 40 nM CTB-A647. Inverted grayscale images of Sec61a-EGFP for the entire cell (far Left, bar = 10μm), 3-color merge and grayscale images of the individual channels (right panels, bar = 10μm).

B: Fraction of MEF-GM1$^{-/-}$ cells showing Sec61/ER colocalization for Alexa-labeled C16:1 and C16:0 following CTB treatment for 5 hours. n = 112 and 83 cells counted respectively.

C: Experiments performed as in (B) but with no CTB crosslinking.

D: Doses probed for each unlabeled GM1 isoform incorporated into the PM of MEF-GM1$^{-/-}$ cells as measured by enzymatic assay for surface-bound CTB-HRP conjugate. Cells were incubated with 20 nM CTB-HRP to label the PM at 4°C. Filled-bars indicate the conditions used in subsequent studies to load cells equally (red dotted line). (mean ± SEM, N = 3)

E: Fraction of MEF-GM1$^{-/-}$ cells showing Sec61/ER colocalization for unlabeled C16-GM1 variants following 20 nM CTB-Alexa594 treatment for 5 hours.

F: Time course of toxin-induced intracellular cAMP production in MEF-GM1$^{-/-}$ cells. (mean ± SEM, N = 3)

Bar graphs in B, C & E show mean ± SEM for N = 3 independent scores.

See also Figure S4.

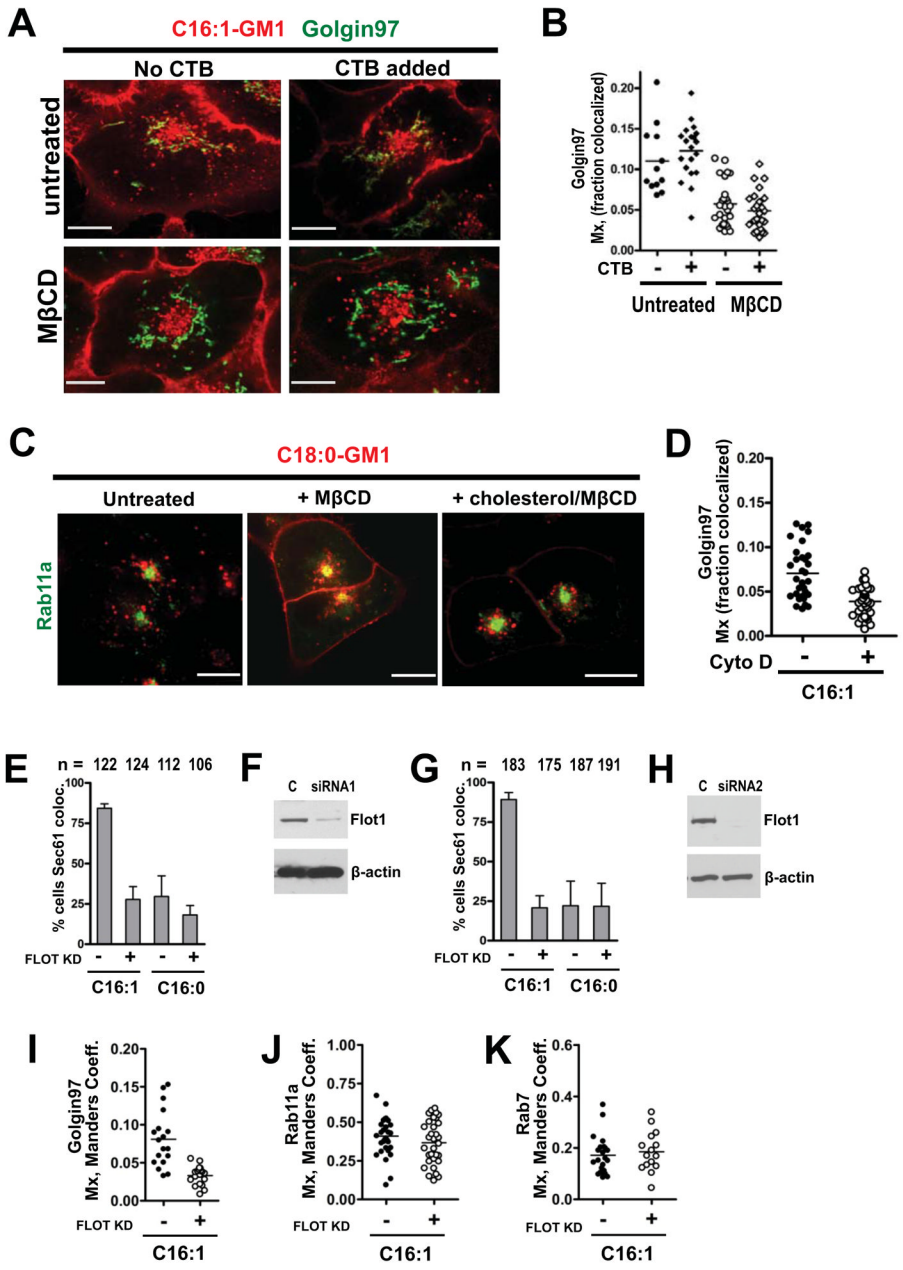

Figure 7. Retrograde trafficking for the unsaturated C16:1-GM1 species depends on cholesterol, actin and flotillin-1

A: A431 cells expressing Golgin97-EGFP were depleted of membrane cholesterol with 5 mM MβCD (bottom panels), or not treated (top panels) and loaded with Alexa-labeled C16:1-GM1 followed by treatment with 40 nM CTB.

B: Histogram quantitating the colocalization of C16:1-GM1 with Golgin97 in cholesterol depleted (right columns), or control (left columns) cells treated or not with CTB. Each data point represents a field of view containing 2–3 cells on average.

C: Alexa568 C18:0-GM1 was loaded into A431 cells expressing Rab11-EGFP that were untreated (left panel – $M_x = 0.05$) or treated with MβCD (middle panel - $M_x = 0.13$). Panel to right shows cholesterol depleted cells repleted with cholesterol $M_x = 0.05$. N = 43 cells analyzed per treatment.

D: Histograms quantitating the fraction of C16:1-GM1 colocalizing with the TGN in Golgin97 – expressing A431 cells pre-treated with 20 μM cytochalasin D to depolymerize actin.
E: Fraction of A431 cells with C16:1 or C16:0 Alexa GM1 colocalized in Sec61-EGFP ER/nuclear envelope. Cells transfected with flotillin-1 siRNA and control siRNA were studied and scored by three investigators blinded to treatment groups.
F: Representative immunoblot probed with mouse antibody against flotillin-1 or β-actin in A431 cell lysates.
G & H: same as in panels (E) and (F) using siRNA against flotillin-1 obtained from a different source.
I – K: Histograms quantitating colocalization of the C16:1 Alexa-GM1 isoform with Golgin97 (I), Rab11a (J) and Rab7 (K) in cells transfected with Flotillin1 siRNA (open circles), or untransfected controls (closed circles).
(Bar graphs show mean ± SEM, N = 3 independent scores.)